UK Atomic Energy Authority

UKAEA-STEP-PR(22)02

F. Schoofs, T. N. Todd

Magnetic field and power consumption constraints for compact spherical tokamak power plants

Magnetic field and power consumption constraints for compact spherical tokamak power plants

F. Schoofs, T. N. Todd

This is a preprint of a paper submitted for publication in
Fusion Engineering and Design

Magnetic field and power consumption constraints for compact spherical tokamak power plants

F. Schoofs*, T. N. Todd

United Kingdom Atomic Energy Authority, Culham Centre for Fusion Energy, Culham Science Centre, Abingdon, Oxon, OX14 3DB, UK

Abstract

We describe a workflow that is able to approximate basic machine parameters (including but not limited to plasma current I_p, major radius R_0, toroidal magnetic field B_0, fusion power P_fusion) based on the choice of maximum field $B_\mathrm{TF,max}$ on the in-board leg of the toroidal field (TF) coil of a spherical tokamak (ST) fusion power plant (FPP), its aspect ratio A, the distance between the in-board TF leg and the plasma edge and a limited set of plasma physics parameters typical for an ST FPP. Together with an estimation of the electrical power exported as a function of the fusion gain Q, this allows the mapping of the parameter space where such power plants can be compact while still being commercially viable.

Keywords: spherical tokamak, fusion power plant

1. Introduction

Spherical tokamak (ST) fusion power plants (FPP) have been proposed as more compact devices for fusion power generation than conventional tokamaks [1–6], due to beneficial plasma physics effects [7]. However, rather than starting from the ideal plasma scenario, it is possible to bound the design space, based on engineering constraints and physics approximations [8–10].

In any magnetic confinement device, the magnets play a crucial role, with the Toroidal Field (TF) magnets providing the dominant plasma confinement field in tokamaks and stellarators. For practical tokamak TF magnets, Nb_3Sn is used for ITER [11], KSTAR [12] and planned for EU-DEMO [13], while for CFETR both a Nb_3Sn-NbTi graded hybrid coil [14] and a REBCO coil [15] are being considered. A REBCO-Nb_3Sn-NbTi graded coil has been proposed for the EU-DEMO central solenoid [16].

Here we consider the implications of the peak field at the in-board leg of the TF coil on the major radius and on-axis magnetic field of ST FPPs and

*Corresponding author: frank.schoofs@ukaea.uk

the resulting estimated power gain Q, here estimated based on ITER-98(y,2) scaling. The necessary recycled power to support the plasma in steady state, together with estimates of the power required for the balance of plant on the fusion reactor site, are also considered in order to select a parameter range that could provide commercially relevant electricity output to the grid. Rather than aiming for accurate machine design points, the purpose is to elucidate trends and identify regions of interest in the design parameter space, which can then be further refined in system design codes, such as PROCESS [10, 17], MIRA [18] or BLUEPRINT [19].

2. Implications of the centre column radial build for the plasma major radius

The outermost edge of the inboard leg of the TF magnet $R_{\mathrm{TF,in}}$ is determined by the allowed peak field $B_{\mathrm{TF,max}}$ on the magnet conductor and the total current in all TF coils (sometimes called the 'rod current') I_{TF}:

$$R_{\mathrm{TF,in}} = \frac{\mu_0 I_{\mathrm{TF}}}{2\pi B_{\mathrm{TF,max}}} \tag{1}$$

It is possible to add to this radius of the TF conductor stack an estimate of a realistic total radial build thickness t_{inboard} which includes the thermal insulation, the vacuum barrier, the neutron shield, cooling (or heat extraction) channels, plasma facing components and their supporting structure, and a vacuum gap to the last closed flux surface to accommodate plasma position control errors and the scrape-off layer. Special inboard divertor or limiter flux expansion provisions have not been considered here but could be accommodated by raising the thickness of the total radial build, perhaps considered as additional inboard gap since they would not contribute significantly to the neutron shielding of the centre column. This then sets the inboard radius of the plasma R_{inboard}, so a prescription of plasma aspect ratio A then sets the major radius R_0 as

$$R_0 = \frac{R_{\mathrm{inboard}}}{1 - \frac{1}{A}} = \frac{R_{\mathrm{TF,in}} + t_{\mathrm{inboard}}}{1 - \frac{1}{A}} \tag{2}$$

and the vacuum field at the geometric centre of the plasma as:

$$B_0 = \frac{\mu_0 I_{\mathrm{TF}}}{2\pi R_0} = \frac{R_{\mathrm{TF,in}}}{R_0} B_{\mathrm{TF,max}} \tag{3}$$

ignoring ripple due to the finite number of TF coils [14].

The aspect ratio of an ST FPP should clearly be chosen in the ST-range, i.e. $A < 2$ [7], although an optimal power plant configuration is likely to have $A > 1.4$ [20]. If $A \leq\sim 1.8$, it might be possible that no in-board blanket is required to achieve a Tritium Breeding Ratio (TBR) of > 1. This is due to the relatively small solid angle presented to the neutrons by the centre column in a low-aspect ratio tokamak, compared to that presented by its outer wall, as discussed more fully in [9]. Existing and proposed ST FPP machine designs have aspect ratios in the 1.5-1.8 range [1–5, 21]. Here we choose $A = 1.8$, although our analysis is valid for any chosen value of A, apart from increasing the inboard shield thickness to $\sim$1.1 m to achieve both adequate shielding and tritium breeding for $A > 1.9$.

In the following analysis, the total thickness of the mid-plane radial build, going from the outer radius of the TF central conductors $R_{\mathrm{TF,in}}$ to the inboard edge of the plasma, t_{inboard}, is chosen as 0.85 m. This is based on estimations of:

- 50 mm thermal insulation;

- 200 mm vacuum barrier, scaling down from ITER's double wall thickness of ∼300 mm [22, 23], allowing for a more favourable aspect ratio of this cylindrical part of the vessel and the option for a higher strength structural material;
- 550 mm of neutron shielding, including structural material and cooling provisions;
- a nominal 50 mm plasma gap, defined as the distance between the first wall and the inner plasma boundary, as defined by the last closed flux surface, the separatrix in a divertor configuration, otherwise the first flux surface intercepted by a physical structure;

The most critical of these is the thickness of neutron shielding, which for optimised elemental combinations provides one decade of attentuation of the neutron flux per 130–150 mm of shield thickness [24–29]. Accordingly, the material selection and desired lifetime of the shielded components allows some variation of this part of the radial build. The suggested 550 mm of neutron shielding (with e.g. $Zr(BH_4)_4$, W or WC), together with the roughly one decade of neutron flux attenuation accorded by the 200 mm of vacuum vessel wall [22, 30], provides about five decades of neutron flux attenuation and is chosen to allow a few full power years of FPP operation before significant degradation of the superconductor or its potting compound and also to limit the neutronic heating load on the cryogenic system to acceptable values [31–34]. This is important because the cryogenic system is generally found to represent a significant demand on the 'Balance of Plant' (BoP) recycled power of the reactor [35–38].

3. Projections for plasma current & power gain

At this point, given a choice of peak B_{TF}, an in-board radial build thickness $R_{\mathrm{TF,in}} + t_{\mathrm{inboard}}$ and aspect ratio A, the plasma parameters R_0, minor radius a and on-axis magnetic field B_0 are essentially determined.

Estimating an approximate plasma current I_{p} is also possible by noting that the maximum plasma elongation κ that is reliably controllable, is in the vicinity of 1.6–2.0 times the natural elongation κ_{nat} in the neutrally stable situation of a pure vertical field [39, 40]. A significant bootstrap current fraction is typically intended in ST FPP concepts [40–42], making the plasma current profile somewhat broad or even hollow, and hence the internal inductance l_{i} quite small. The value of the bootstrap current fraction coefficient, C_{BS}, used or implied in those studies is consistent with values of l_{i} well below 0.6 [43], but a more conservative value of 0.6 is used to estimate the natural elongation in this work. References [44–46] closely agree with the relationship from [47]:

$$\kappa_{\mathrm{nat}} \approx 1 + (\frac{0.6306}{l_i} + \frac{0.1064}{l_i^2})A^{-2} + (\frac{0.1952}{l_i} - \frac{0.2439}{l_i^2})A^{-4} \tag{4}$$

Thus, a reasonable estimate for the elongation κ_{95} of the poloidal flux surface containing 95% of the poloidal flux change from the minor axis of the plasma to the last closed surface, with good feedback control of the vertical position, is:

$$\kappa = \kappa_{95} \approx 1.8\kappa_{\mathrm{nat}} \tag{5}$$

Neglecting the small effects of triangularity and toroidicity, and using the first order elliptical integral of the ellipsoidal poloidal circumference of the plasma, this leads to estimates for the plasma volume V_{plasma} (in m^3) and the toroidal surface area A_{plasma} (in m^2):

$$V_{\mathrm{plasma}} = 2\pi^2 R_0 a^2 \kappa \tag{6}$$

$$A_{\mathrm{plasma}} = 4\pi^2 R_0 a \sqrt{(\frac{1+\kappa^2}{2})} \tag{7}$$

Given the estimate of plasma elongation, the plasma current I_{p} (in MA) can also be estimated from [7, 48]:

$$I_{\mathrm{p}} = \frac{5aB_0}{Aq_{95}} \frac{(1.17 - 0.65/A)}{\left(1 - \frac{1}{A^2}\right)^2} \frac{\left(1 + \kappa^2\left(1 + 2\delta^2 - 1.2\delta^3\right)\right)}{2} \tag{8}$$

with triangularity δ, safety factor q_{95}, a in m and B_0 in T. For reliable operation, higher values (> 5) of q_{95} are more appropriate for an ST FPP [7, 49], compared to values of $\sim$3 preferred for $A \sim 3$ tokamaks. Operating data for MAST [50, 51] suggest a q_{95} in the range 5–10.

Moving towards a scaling to determine the fusion power, a conservative approach to energy confinement scaling is adopted by noting that START, NSTX and MAST data fit reasonably well to the canonical ITER-98(y,2) scaling [52–54]. It is possible to estimate the line average electron density $\overline{n_{\mathrm{e}}}$ (in units

of $10^{20}/\mathrm{m}^3$) required for that scaling as a fraction $f_{\mathrm{Greenwald}}$ of the Greenwald density n_{G}. For the range of indexed parabolae used as the profile class here, namely:

$$n_{\mathrm{e}} = n_{\mathrm{e},0}\left(1-\rho^2\right)^{\alpha_{\mathrm{n}}} \tag{9}$$

with $\rho = r/a$ and the density profile peaking factor $0.1 \leq \alpha_{\mathrm{n}} \leq 2$, the central electron density $n_{\mathrm{e},0}$ can be approximated as a function of the line-averaged electron density $\overline{n_{\mathrm{e}}}$, to within less than 1%, by:

$$n_{\mathrm{e},0} = \overline{n_{\mathrm{e}}}\left(1+\alpha_{\mathrm{n}}\right)^{0.58} \tag{10}$$

Hence:

$$\begin{aligned} n_{\mathrm{e},0,20} &= f_{\mathrm{Greenwald}} n_{\mathrm{G}}\left(1+\alpha_{\mathrm{n}}\right)^{0.58} && (11)\\ &= f_{\mathrm{Greenwald}} \frac{I_{\mathrm{p}}}{\pi a^2}\left(1+\alpha_{\mathrm{n}}\right)^{0.58} && (12) \end{aligned}$$

where $n_{\mathrm{e},0,20}$ is the central density in units of 10^{20} m^{-3}, I_{p} in MA and a in m.

It is possible to express the stored kinetic energy in the plasma W in two ways, using the central ion temperature $T_{\mathrm{i},0}$ as the solved variable in our analysis. The first expression is based on the confinement time, here taken from ITER-98(y,2) [55, 56], although other scalings can be applied [6, 57–59]:

$$\begin{aligned} W &= P_{\mathrm{transp}}\tau_{E,\mathrm{ITER\text{-}98(y,2)}} && (13)\\ &= 0.0562 H P_{\mathrm{transp}}^{0.31} B_0^{0.15} I_p^{0.93} \kappa^{0.78} n_{\mathrm{e},19}^{0.41} a^{0.58} R_0^{1.39} M^{0.19} && (14) \end{aligned}$$

with W in MJ, I_{p} in MA, B_0 in T, n_{e} the average electron density now in $10^{19}\mathrm{m}^{-3}$ and M the atomic mass of the plasma fuel in AMU. For a 50-50 D-T mixture, $M = 2.5$. The transported power P_{transp} can be expressed as:

$$\begin{aligned} P_{\mathrm{transp}} &= P_{\mathrm{alpha}} + P_{\mathrm{aux}} - P_{\mathrm{radiated\text{-}core}} && (15)\\ &= \left(P_{\mathrm{alpha}} + P_{\mathrm{aux}}\right)\left(1 - f_{\mathrm{radiated\text{-}core}}\right) && (16)\\ &= P_{\mathrm{fusion}}\left(0.2 + 1/Q\right)\left(1 - f_{\mathrm{radiated\text{-}core}}\right) && (17) \end{aligned}$$

The fusion power P_{fusion} (in MW) is itself a function of $T_{\mathrm{i},0}$ and depends on the D-T reactivity (i.e. the D-T reaction cross-section σ averaged over a Maxwellian distribution of the centre of mass velocity v of the colliding ion fuel species, which are assumed to have the same temperature), for which a fit can be found in [60] and is given by the volume integration:

$$\begin{aligned} P_{\mathrm{fusion}} &= E_{\mathrm{fusion}} \int_{\mathrm{V}} n_{\mathrm{D}} n_{\mathrm{T}} < \sigma v > d\mathrm{V} && (18)\\ &= E_{\mathrm{fusion}} \frac{n_{\mathrm{e},0}^2}{4}\left(\frac{Z_{\mathrm{i}} - Z_{\mathrm{eff}}}{Z_{\mathrm{i}} - 1}\right)^2 \frac{< \sigma v > (T_{\mathrm{i},0}) V_{\mathrm{plasma}}}{1 + 2\alpha_{\mathrm{n}} + \alpha_{<\sigma v>}} && (19) \end{aligned}$$

where the term in $Z_{\rm i}$ and $Z_{\rm eff}$ accounts for fuel dilution by a notional single impurity of charge $Z_{\rm i}$, creating an average charge of $Z_{\rm eff}$. This modifies the expression that would apply for a pure D-T plasma with $n_{\rm D} = n_{\rm T} = n_{\rm e}/2$. The term in $\alpha_{\rm n}$ and $\alpha_{<\sigma v>}$ accounts for the integration of the product of the indexed parabolae representing profile peaking. In this equation $E_{\rm fusion} = 17.6 \cdot 10^6$ e (J) with e being the elementary electron charge. The peaking factor $\alpha_{<\sigma v>}$ can be approximately expressed as a function of the temperature profile peaking factor $\alpha_{\rm T}$ using a fit to the numerical integration of the $<\sigma v>$ profile for an appropriate range of $\alpha_{\rm T}$ describing the temperature profile $T = T_0 \left(1 - \rho^2\right)^{\alpha_{\rm T}}$:

$$\alpha_{<\sigma v>} \approx 1.26 \log \left(\frac{100}{T_{\rm i,0}} \right) \alpha_{\rm T} \tag{20}$$

The coefficients in (20) were chosen to suit significantly peaked reactivity profiles, i.e. those with $T_{\rm i,0} < 65$ keV or with $\alpha_{\rm T} > 1.5$, which are typical of the solutions of interest.

The second expression for the stored kinetic energy, ignoring the non-thermal α particle population, and assuming that $T_{\rm i} = T_{\rm e}$ (in eV), is given by:

$$W = \frac{3}{2} V_{\rm plasma} \int_V \left(n_{\rm e,i} T_{\rm e,i} \right) {\rm d}v \tag{21}$$

$$\approx V_{\rm plasma} \left(\frac{1 + 2Z_{\rm i} - Z_{\rm eff}}{2Z_{\rm i}} \right) \frac{3 e n_{\rm e,0} T_{\rm i,0}}{1 + \alpha_{\rm n} + \alpha_{\rm T}} \tag{22}$$

where the subscript (e,i) implies summing over electrons and ions and the factor involving $Z_{\rm i}$ and $Z_{\rm eff}$ accounts for the reduction in total ion density due to the lumped impurity species $Z_{\rm i}$.

Based on preset values for the plasma and engineering parameters, including $R_{\rm TF,in}$ and Q, we can now numerically calculate the value of $T_{\rm i,0}$ which satisfies the simultaneous equations (14) and (22) and is in a realistic reactor range (i.e. below 65 keV). This then provides a value for $P_{\rm fusion}$ with (19) and for the normalised ratio (in %) of plasma pressure and magnetic pressure, $\beta_{\rm N}$, [61] with:

$$\beta_{\rm N} = \beta_T \left(\frac{a B_0}{I_{\rm p}} \right) \tag{23}$$

$$= 2 n_{\rm e,0} \left(\frac{1 + 2Z_{\rm i} - Z_{\rm eff}}{2Z_{\rm i}} \right) \left(\frac{e T_{\rm i,0}}{1 + \alpha_{\rm n} + \alpha_{\rm T}} \right) \left(\frac{2\mu_0}{B_0^2} \right) \left(\frac{a B_0}{I_{\rm p}} \right) \tag{24}$$

with $T_{\rm i,0}$ in eV. Typically the value of $\beta_{\rm N}$ is found to be lower than 2.8 for low-n kink modes with no conducting wall close to the plasma [62, 63] and in standard aspect ratio tokamaks it is generally less than 4 for ballooning modes where there is such a wall [64, 65], although both limit values depend significantly on the plasma current and pressure profiles. Experimentally $\beta_{\rm N}$ values of up to ~6 (or 10–13·$l_{\rm i}$) have been achieved in NSTX and in MAST [50, 51, 66–68]. Using $\beta_{\rm N}$, it is possible to calculate the bootstrap current fraction $f_{\rm BS}$:

$$f_{\rm BS} = 0.05 q^* \beta_{\rm N} A^{0.5} C_{\rm BS} \tag{25}$$

with $q^* = 2.5aB_0(1+\kappa^2)/(AI_\mathrm{p})$ and C_BS calculated from the fit provided in [43]. The required current drive power P_CD is then:

$$P_\mathrm{CD} = n_{\mathrm{e},20} R I_\mathrm{p} (1 - f_\mathrm{BS})/\gamma_\mathrm{CD} \tag{26}$$

where γ_CD is the efficiency of the current drive, which can be up to 0.36 $\mathrm{MA/m^2MW}$ [69, 70].

The average neutron wall loading Γ_n in $\mathrm{MW/m^2}$ can be estimated from:

$$\Gamma_\mathrm{n} = \frac{P_\mathrm{fusion}}{1.1 A_\mathrm{plasma}} \left(\frac{14.06}{17.6} \right) \tag{27}$$

where the factor 1.1 allows for the plasma gap. Given a safe level of neutron wall loading or desired first wall lifetime in $\mathrm{MWyrs/m^2}$ (e.g. related to neutron damage, activation or reduced tritium breeding capability), designers can use these values to limit solutions to cases respecting that limit or that lifetime in full power years.

A similar calculation can be made to estimate the total fast neutron flux ($E > 0.1$ MeV) on the central TF conductor stack, and thus its lifetime, based on an upper limit of $\sim 3 \cdot 10^{22}$ $\mathrm{n/m^2}$ [71, 72]. Assuming that the fast flux is 6–8 times the 14 MeV flux determined by the fusion power (as can be inferred from the analyses in [30, 73]) over ∼1.1 times the plasma surface area and assuming an order of magnitude in attenuation per 0.13 m of inboard shield thickness t_shield [26, 28, 29], this results in a lifetime (in seconds) of:

$$t_\mathrm{life,SC} = \frac{3 \cdot 10^{22}}{10^{-(t_\mathrm{shield}/0.13)}} \frac{1.1 A_\mathrm{plasma}}{6 P_\mathrm{fusion} / \left(17.6 \cdot 10^6 e\right)} \tag{28}$$

with e the elementary electron charge, P_fusion here in W and noting that t_shield (in m) is approximately 0.3 m less than t_inboard as defined in section 2. As for the first wall, this criterion could be used to select solutions meeting a chosen TF central conductor lifetime.

Finally, it is possible to implement plasma physics checks to confirm that returned solutions are self-consistent, namely that:

1. the required current drive power P_CD is less than $P_\mathrm{aux} = P_\mathrm{fusion}/Q$;
2. the confinement time from the scaling in (14) does not exceed the confinement time from purely ohmic heating taken as $\tau_\mathrm{E,OH} = 0.075 n_{\mathrm{e},20} q^* a R_0^2$, close to the upper bound of the data in Figure 28 of [74], and broadly consistent with the upper bound of other OH experiments including JET [75];
3. the asserted radiated power $f_\mathrm{radiated\text{-}core} P_\mathrm{fusion}(0.2 + 1/Q)$ is higher than the sum of the bremsstrahlung [76] and synchrotron losses [77], thus leaving a margin for balancing the total core loss power by controlled additional radiative losses from impurity line radiation;
4. the transported power P_transp is greater than the H-mode threshold power scaling [56].

Many of the approximations used in this heuristic analysis could be refined to allow for more realistic design optimisations, plasma physics and control assumptions, but the resulting description of the fusion plasma is considered to be sufficiently accurate for the trends that this work endeavours to demonstrate.

4. Dependence of the electrical power exported on Q

An important consideration is the value of Q necessary for an ST FPP to be commercially viable, which depends on the fraction of electricity exported to the grid. For the calculation below we assume superconducting magnets for the machine, reducing the electrical demand, both for the magnet power supplies and the cryoplant.

The electrical power demand of the auxiliary heating $P_{\mathrm{aux,el}}$ (plasma heating & current drive power, ignoring transmission losses) can be expressed as:

$$P_{\mathrm{aux,el}} = \frac{P_{\mathrm{fusion}}}{\eta_{\mathrm{aux,wall}} Q} \tag{29}$$

where η_{wall} is the wall-plug efficiency of the current drive and external heating systems, which can be ∼40% [38]. This $\eta_{\mathrm{aux,wall}}$ is defined as the power absorbed by the plasma with respect to the power drawn from the electrical supply. Different heating systems have different efficiencies, e.g. approximately 30-45% for LHCD and ECRH [78], 40–50% for ICRH [78, 79] (with possible scope to 69% [80]) but as low as 20–30% for Neutral Beam Injectors (NBI) [78]. There is ongoing work to increase NBI efficiency to 40–60%, which is the target for EU-DEMO [81, 82]. High-efficiency (65-90%) klystron designs also exist [83]. Here we adopt a plausible target of 40%.

If we assume that the first wall and divertor heating power could be removed at a high temperature similar to that of the blanket and shield heating, the total electrical power $P_{\mathrm{total,el}}$ with a fusion power fraction of 80% from neutrons and 20% from alpha particles can be approximated as

$$\begin{aligned} P_{\mathrm{total,el}} &= \eta_{\mathrm{generator}} P_{\mathrm{thermal}} && (30)\\ &= \eta_{\mathrm{generator}} \left(P_{\mathrm{thermal,blanket}} + P_{\mathrm{thermal,divertor}} + P_{\mathrm{aux,th}} \right) && (31)\\ &= \eta_{\mathrm{generator}} P_{\mathrm{fusion}} \left(0.8 M_{\mathrm{EMF}} + 0.2 + Q^{-1} \right) && (32) \end{aligned}$$

The thermal-to-electric conversion efficiency $\eta_{\mathrm{generator}}$ is typically 35% to 37.5% [38, 84], though alternative approaches might reach 45-50% [85]. M_{EMF} is the neutron Energy Multiplication Factor, which ranges between 0.9-1.35 [86], and specifically 1.2-1.4 for FPP-relevant blanket configurations [87, 88] and ∼ 1.4 for steel in the divertor structure [89]. Here we assume an average $M_{\mathrm{EMF}} = 1.2$.

There are many analyses of the electrical power $P_{\mathrm{BoP,el}}$ required for the Balance of Plant (BoP) of a fusion power plant in the literature, each with a different subset of plant systems and losses considered. Here BoP is taken to mean all the recycled power required for reactor operation, including the primary heat extraction system coolant circulators but excluding the plasma auxiliary heating and current drive systems, which here are treated separately. Example values of the fraction of generated electricity required for the BoP, f_{BoP}, vary widely, broadly reducing as Q rises and including 6% for STARFIRE [87], ∼30% for ARC [85], ∼64% for DEMO [38], 40–50% for CFETR [90] and an equivalent value of 46% for ITER [35]. STARFIRE, ITER and DEMO are

the most comprehensive of these examples, but none of them address all the plant demands collectively considered by all of them. We consider a value of $f_{\mathrm{BoP}} = 35\%$ of the gross electrical generated power a reasonable target for an optimised, commercial FPP.

The fraction of exported electricity f_{export}, relevant for a commercial FPP would be:

$$f_{\mathrm{export}} = 1 - \frac{P_{\mathrm{aux,el}} + P_{\mathrm{BoP,el}}}{P_{\mathrm{total,el}}} \tag{33}$$

We can now substitute (29) and (32) in (33) to yield:

$$f_{\mathrm{export}} = 1 - \frac{\frac{P_{\mathrm{fusion}}}{\eta_{\mathrm{aux,wall}} Q} + f_{\mathrm{BoP}} \left[\eta_{\mathrm{generator}} P_{\mathrm{fusion}} \left(0.8 M_{\mathrm{EMF}} + 0.2 + Q^{-1}\right)\right]}{\left[\eta_{\mathrm{generator}} P_{\mathrm{fusion}} \left(0.8 M_{\mathrm{EMF}} + 0.2 + Q^{-1}\right)\right]} \tag{34}$$

This relationship is graphically shown in Fig. 1, for different values of the fraction f_{BoP}. By comparison, the recycled electricity fraction of AGR [91] and GenIII/III+ [92, 93] fission plants is 3–7% of the gross electrical power output (produced at a thermal-to-electrical efficiency of 30–40%), thus 93–97% if plotted on Fig. 1. Magnetic confinement fusion systems cannot aspire to such high values, largely because of the auxiliary plasma heating and current drive systems, cryoplant and tritium purification and recycling plant that they require. If a commercial FPP aims for an economically conceivable minimum value of 30–40% of gross electrical generation to be exported after allowing for the electrical demand of the plasma heating & current drive systems, then this model suggests that a Q of at least 20–30 would be required.

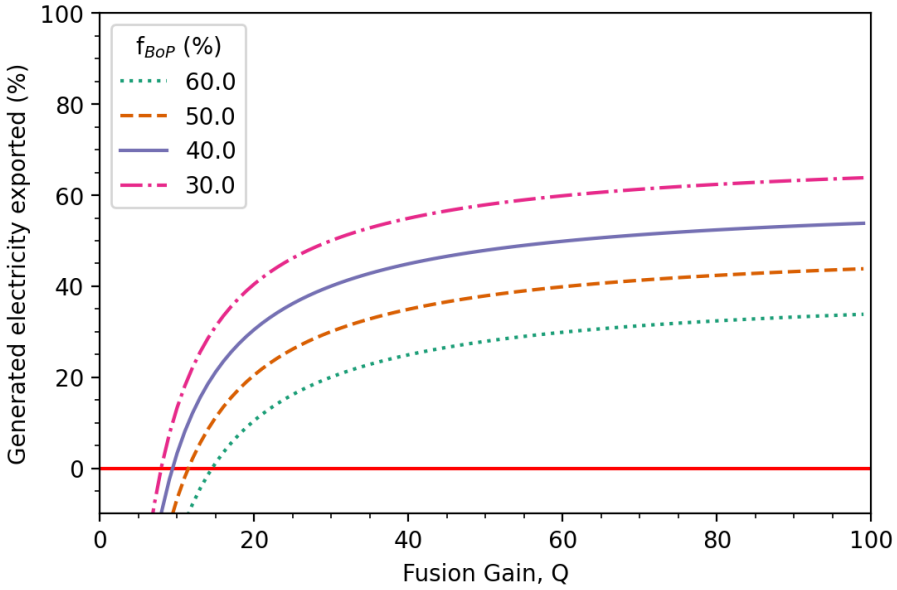

Figure 1: Fraction of exported electricity as a function of Q for different fractions f_{BoP} of $P_{\mathrm{total,el}}$, based on eq. (34).

5. ST FPP reactor parameters

A plot can now be made for the various machine and plasma parameters that are an immediate consequence of the choice of permissible peak field $B_{\mathrm{TF,max}}$, in-board radial build thickness $R_{\mathrm{TF,in}} + t_{\mathrm{inboard}}$ and Q, as well as other plasma parameters appropriate for an ST FPP. The values selected in this study are listed in Table 1 and the code is available online [94]. Multiple reactor configurations are possible, but only those that satisfy the plasma physics checks (see section 3) and the neutron wall loading limit and that produce net electrical output are retained. It should be noted that no specific superconductor characteristics are used to obtain these results.

It may be necessary to select a larger $R_{\mathrm{TF,in}}$, e.g. depending on the choice of superconductor for the TF coil or to accommodate structural support. Even with state-of-the-art high-field capability, the achievable current density of Nb_3Sn [95] is outperformed by REBCO [96], which has been demonstrated with a 45.5 T magnet insert [97]. For example, the highest achievable engineering current density at 4.2 K and 20 T for an HTS REBCO tape can be as high as 3620 MA/m^2 [96], whereas well-optimised Nb_3Sn strand would only achieve 274 MA/m^2 [95]. Note that the practical 'cable' engineering current density in the winding pack – allowing for copper or aluminium stabiliser, coolant channels, insulant and any internal support structure – tends to be around 10% of the empirical limit of the strand or tape, based on existing cable designs such as the ITER TF and Central Solenoid Cable-In-Conduit-Conductor [11], HTS CORC 6-around-1 [98] and the HTS VIPER cable [99]. This factor of ∼10% can be greatly improved if a non-insulating, reduced-stabiliser winding is in mind (as used in the 45.5 T insert in [97]), although that would introduce problems of both restricted current ramping speed and quench protection. All superconductors exhibit reducing critical current for increasing magnetic field strength, so that grading the current density to be highest in the lowest field region would permit the winding pack to be thinner with the same superconducting margin as a constant current density coil would have in its peak field region. For a TF central conductor stack, this could provide more space for an inboard solenoid winding if the mechanical stresses in the winding pack and the support structures were acceptable, or simply permit a smaller $R_{\mathrm{TF,in}}$ to be realised if required.

Fig. 2a–d show contour plots of the exported electric power for valid reactor results for Q values of 10, 20, 30 and 40 respectively as a function of $R_{\mathrm{TF,in}}$ (and thus R_0 for the chosen A (1.8) and t_{inboard}) and $B_{\mathrm{TF,max}}$. While $Q = 10$ machines could be compact designs at higher peak magnetic fields (i.e. exceeding 15 T), exporting several hundreds MW of electrical power, the derivation in section 4 shows that these are unlikely to be attractive commercially. The range of valid reactor configurations at each Q is determined by three limitations: at low $B_{\mathrm{TF,max}}$ fields and low R by the condition $P_{\mathrm{CD}} < P_{\mathrm{aux}}$; at low fields and high R by the plasma temperature exceeding 65 keV and at high fields and low R by the neutron wall loading limit $\Gamma_{\mathrm{n,max}}$.

For the remainder of the analysis we focus on the $Q = 20$ solutions, which allow for reasonably compact designs with $R_0 \leq 4$ m. For our chosen aspect ratio

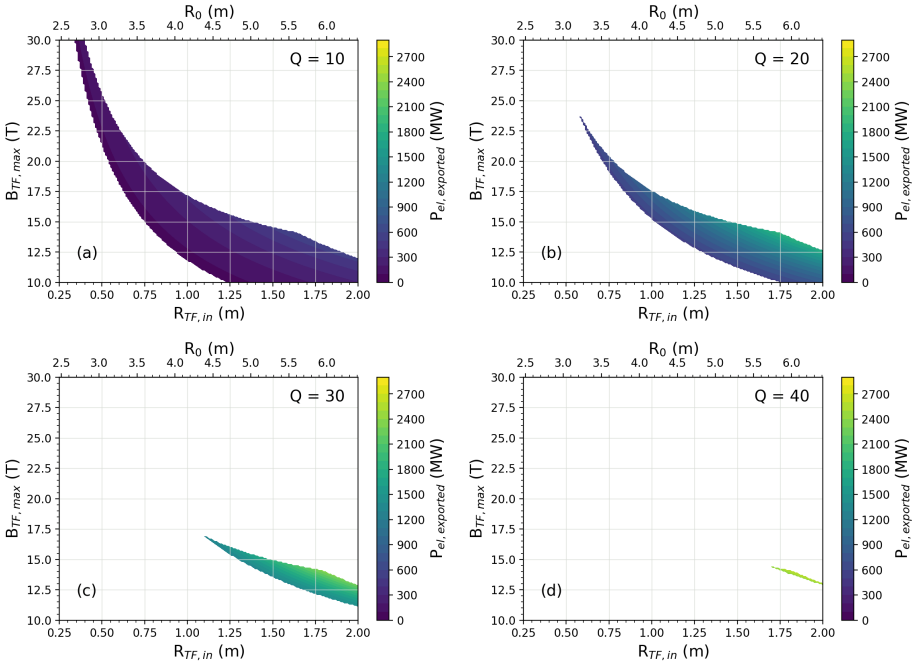

Figure 2: Exported electrical power (in MW) as a function of outer radius of the in-board TF leg $R_{\mathrm{TF,in}}$ and $B_{\mathrm{TF,max}}$ for reactor designs meeting the criteria in Table 1 and for Q values of (a) 10; (b) 20; (c) 30 and (d) 40.

Table 1: Plasma & reactor parameters chosen for the analysis.

Parameter	**Value**
A	1.8
α_{n}	0.2
α_{T}	1.7
δ	0.5
f_{BOP}	35%
$f_{\mathrm{Greenwald}}$	0.9
$f_{\mathrm{radiated\text{-}core}}$	0.4
γ_{CD}	0.36 MA/MW·m^2
$\Gamma_{\mathrm{n,max}}$	5 MW/m^2
H	1.2
$\kappa_{95}/\kappa_{\mathrm{nat}}$	1.8
l_i	0.4
M_{EMF}	1.2
$\eta_{\mathrm{generator}}$	37.5%
$\eta_{\mathrm{aux,wall}}$	40%
q_{95}	10
t_{inboard}	0.85 m
Z_{i}	12
Z_{eff}	1.6

and $\kappa/\kappa_{\mathrm{nat}}$, the plasma volume would exceed that of EU-DEMO if $R_0 > 5.0$ m [100]. Fig. 3a–f show other relevant reactor parameters such as B_0, I_{p}, β_{N}, Γ_{n}, f_{BS} and T_0. The most compact ST FPP designs in this range require magnetic fields on the conductor above 20 T, but the neutron wall loading is close to the Γ_{n} limit, implying shorter in-vessel reactor component lifetimes. An example is given as Variant 1 in Table 2. Variant 2 in the same table can be considered a compromise: more than double the plasma volume, but reduced neutron wall loading and a TF central conductor life approaching 2 full power years (fpy). A more conservative reactor design (Variant 3) would limit $B_{\mathrm{TF,max}}$ to ∼12 T, as in ITER and EU-DEMO, but, even at the smallest radius possible, it will have a consequently larger plasma volume, approaching that of EU-DEMO (2214 m^3, [100]) and having a similar magnitude of exported electric power. In all cases, re-mountable joints would be desired to facilitate the replacement of the inboard leg of the TF magnets. The alternative is to increase the thickness of the neutron shielding to improve the lifetime, at the expense of machine compactness.

Predictions of alternative confinement time scalings can be represented by varying the H factor on the ITER-98(y,2) scaling. For example the equivalent from the ST scaling in Ref. [6] would be $H = 2.27$. In Fig. 4 we have considered a range of solutions for $Q = 20$, with the same engineering and plasma physics parameters as in Table 1, but varying the H factor between 1.0 and 2.5, to reflect the effect of different confinement scalings. It is clear that for increasing H-factors, the machine size decreases significantly for the same net electric

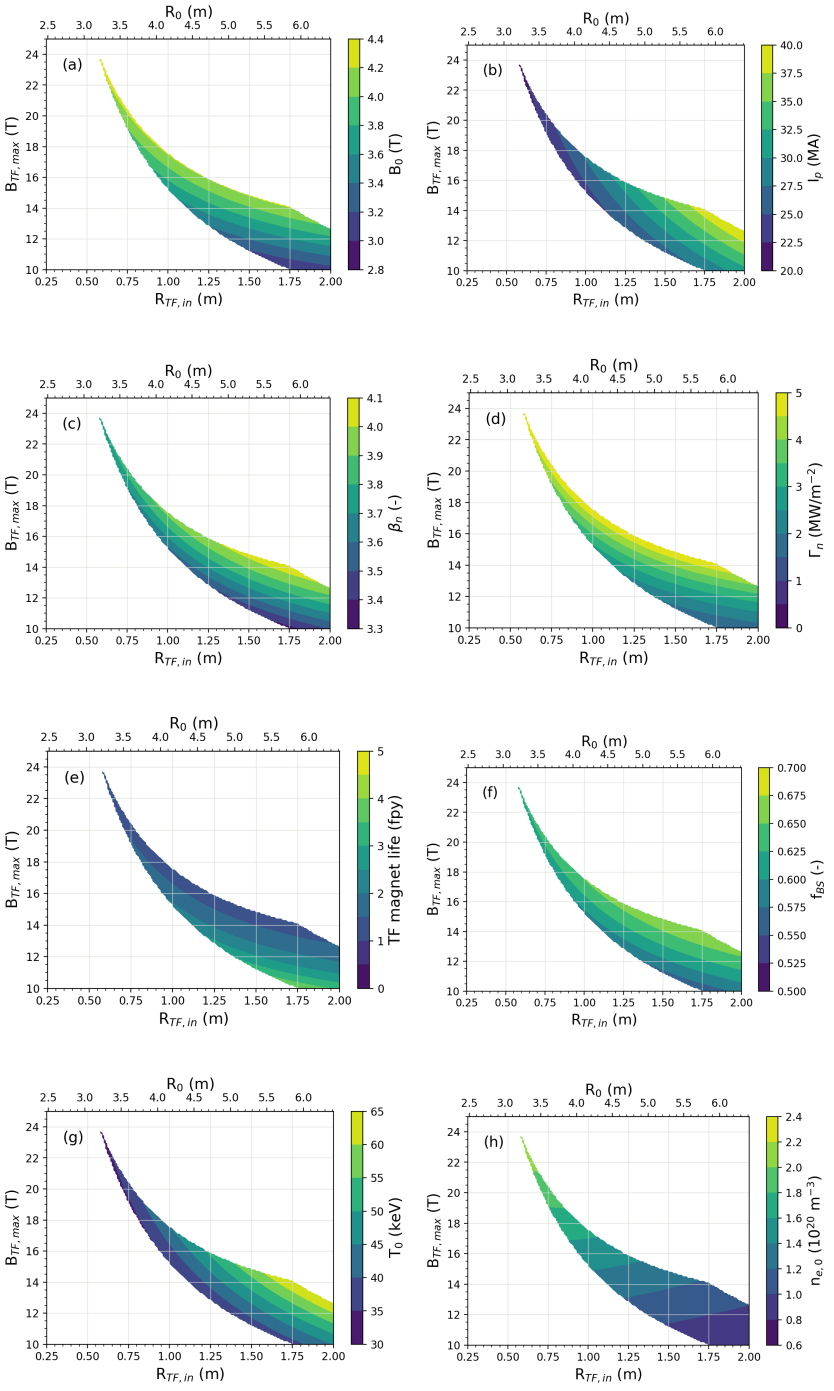

Figure 3: Contour plots of selected reactor parameters as a function of outer radius of the in-board TF leg $R_{\mathrm{TF,in}}$ and $B_{\mathrm{TF,max}}$ for reactor designs meeting the criteria in Table 1 and for $Q = 20$. The parameters are (a) B_0 (T); (b) I_{p} (MA); (c) β_{N}; (d) Γ_{n} (MW/m^2); (e) TF central conductor life (full power years, fpy) (f) f_{BS}; (g) T_0 (keV) and (h) $n_{\mathrm{e},0}$ (10^{20} m^{-3}).

Table 2: Comparison of plasma & reactor parameters for three $Q = 20$ scenarios: most compact (Variant 1), balanced (Variant 2) and conservative (Variant 3). All have the plasma parameters listed in Table 1.

	Variant		
Parameter	**1**	**2**	**3**
$B_{\mathrm{TF,max}}(T)$	23	16	12
$R_{\mathrm{TF,in}}$ (m)	0.6	0.95	1.375
R_0 (m)	3.26	4.05	5.01
B_0 (T)	4.23	3.75	3.30
κ	2.87	2.87	2.87
I_{p} (MA)	22	24	26
$n_{\mathrm{e},0}$ (10^{20} m^{-3})	2.11	1.51	1.07
T_0 (keV)	33	35	37
P_{fusion} (GW)	3.21	3.38	3.37
β_{N}	3.75	3.62	3.47
f_{BS}	0.62	0.60	0.57
P_{CD} (MW)	159	163	165
$P_{\mathrm{total,el}}$ (GW)	1.46	1.54	1.53
$P_{\mathrm{exported,el}}$ (MW)	546	575	573
Plasma volume (m^3)	607	1161	2192
Γ_{n} (MW/m^2)	4.66	3.18	2.07
TF magnet life (fpy)	1.30	1.91	2.93

power output and more radius and magnetic field combinations are available, including at lower neutron wall loading.

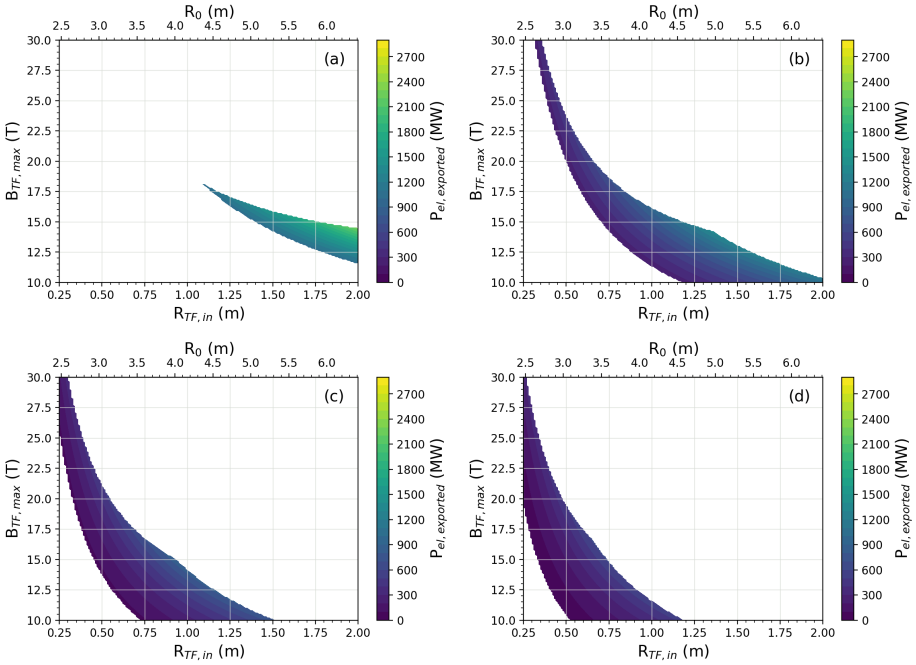

Figure 4: Exported electrical power (in MW) as a function of outer radius of the in-board TF leg $R_{\mathrm{TF,in}}$ and $B_{\mathrm{TF,max}}$ for reactor designs with $Q = 20$ and meeting the criteria in Table 1 with H factor values of (a) 1.0; (b) 1.5; (c) 2.0 and (d) 2.5.

6. Summary

In summary, we have proposed a methodology to infer basic machine and plasma parameters for an ST FPP, based on the peak field on the TF conductor in the centre column and a limited number of physics and engineering assumptions and approximations, endeavouring to respect the established dimensionless operational space of ST experiments [50, 51, 67]. The important impact of the recycled power required for the Balance of Plant has been estimated as part of this assessment. This estimate is intended to cover the electrical demand of all the auxiliary systems required to keep the power plant site operational as well as the primary heat transfer system circulators, considered as additions to the necessary plasma heating & current drive systems. This workflow can, in principle, guide tokamak designers in terms of the realistic parameter space for a power plant more likely to be economically viable, which can subsequently be explored with system design codes. Inevitably the design parameter space is a trade-off between compactness (diameter, plasma volume) and component life time (neutron wall loading). In the cases considered, a sufficient thickness of neutron shielding has been assumed to assure that the TF central conductor stack, including its insulation if present, will serve for several full power years at the specified average neutron wall loading [32–34]. For $Q = 20$ designs, the peak field on the in-board TF conductor needs to be at least 15 T, in order that the net electricity exported to the grid can plausibly achieve a commercially relevant fraction of the gross generated electrical power, while also resulting in ST FPP reactors ($A < 2$) that are significantly more compact in diameter, height and plasma volume than the current EU-DEMO design ($A = 3$, $B_{\mathrm{TF,max}} = 12$ T [100, 101]).

Acknowledgments

This work has been funded by STEP, a UKAEA programme to design and build a prototype fusion energy plant and a path to commercial fusion. To obtain further information on the data and models underlying this paper please contact PublicationsManager@ukaea.uk.

References

[1] G. M. Voss, A. Bond, J. E. Edwards, T. C. Hender, Toroidal field coil design for the spherical tokamak power plant, Fusion Engineering and Design 48 (3) (2000) 407–418. doi:10.1016/S0920-3796(00)00151-4.

[2] H. R. Wilson, J. W. Ahn, R. J. Akers, D. Applegate, R. A. Cairns, J. P. Christiansen, J. W. Connor, G. Counsell, A. Dnestrovskij, W. D. Dorland, M. J. Hole, N. Joiner, A. Kirk, P. J. Knight, C. N. Lashmore-Davies, K. G. McClements, D. E. McGregor, M. R. O'Brien, C. M. Roach, S. Tsaun, G. M. Voss, Integrated plasma physics modelling for the Culham steady state spherical tokamak fusion power plant, Nuclear Fusion 44 (8) (2004) 917–929. doi:10.1088/0029-5515/44/8/010.

[3] A. W. Morris, R. J. Akers, G. F. Counsell, T. C. Hender, B. Lloyd, A. Sykes, G. M. Voss, H. R. Wilson, Spherical tokamaks: Present status and role in the development of fusion power, Fusion Engineering and Design 74 (1) (2005) 67–75. doi:https://doi.org/10.1016/j.fusengdes.2005.08.025.

[4] J. E. Menard, T. Brown, L. El-Guebaly, M. Boyer, J. Canik, B. Colling, R. Raman, Z. Wang, Y. Zhai, P. Buxton, B. Covele, C. D'Angelo, A. Davis, S. Gerhardt, M. Gryaznevich, M. Harb, T. C. Hender, S. Kaye, D. Kingham, M. Kotschenreuther, S. Mahajan, R. Maingi, E. Marriott, E. T. Meier, L. Mynsberge, C. Neumeyer, M. Ono, J.-K. K. Park, S. A. Sabbagh, V. Soukhanovskii, P. Valanju, R. Woolley, Fusion nuclear science facilities and pilot plans based on the spherical tokamak, Nuclear Fusion 56 (10) (2016) 106023. doi:10.1088/0029-5515/56/10/106023.

[5] M. Windridge, Smaller and quicker with spherical tokamaks and high-temperature superconductors, Philosophical Transactions of the Royal Society A: Mathematical, Physical and Engineering Sciences 377 (2019) 20170438. doi:10.1098/rsta.2017.0438.

[6] A. E. Costley, S. A. M. McNamara, Fusion performance of spherical and conventional tokamaks: implications for compact pilot plants and reactors, Plasma Physics and Controlled Fusion 63 (2021) 035005. doi:10.1088/1361-6587/abcdfc.
URL `https://doi.org/10.1088/1361-6587/abcdfc`

[7] Y.-K. Peng, D. Strickler, Features of spherical torus plasmas, Nuclear Fusion 26 (6) (1986) 769–777. doi:10.1088/0029-5515/26/6/005.

[8] J. P. Freidberg, F. J. Mangiarotti, J. Minervini, Designing a tokamak fusion reactor - How does plasma physics fit in?, Physics of Plasmas 22 (7) (2015). doi:10.1063/1.4923266.

[9] J. E. Menard, Compact steady-state tokamak performance dependence on magnet and core physics limits, Philosophical Transactions of the Royal Society A: Mathematical, Physical and Engineering Sciences 377 (2019) 20170440. doi:10.1098/rsta.2017.0440.

[10] S. I. Muldrew, H. Lux, G. Cunningham, T. C. Hender, S. Kahn, P. J. Knight, B. Patel, G. M. Voss, H. R. Wilson, 'PROCESS': Systems studies of spherical tokamaks, Fusion Engineering and Design 154 (2020) 111530. doi:10.1016/j.fusengdes.2020.111530.

[11] L. Muzzi, G. De Marzi, A. Di Zenobio, A. Della Corte, Cable-in-conduit conductors: Lessons from the recent past for future developments with low and high temperature superconductors, Superconductor Science and Technology 28 (5) (2015) 053001. doi:10.1088/0953-2048/28/5/053001.

[12] G. S. Lee, S. M. Hwang, C. S. Chang, H. Y. Chang, M. H. Cho, B. H. Choi, Et.al., The KSTAR project : An advanced steady state superconducting tokamak experiment, Nuclear Fusion 40 (3Y) (2000) 575–582.
URL http://dx.doi.org/10.1088/0029-5515/40/3Y/319

[13] V. Corato, T. Bagni, M. E. Biancolini, R. Bonifetto, P. Bruzzone, N. Bykovsky, D. Ciazynski, M. Coleman, A. della Corte, A. Dembkowska, A. Di Zenobio, M. Eisterer, W. H. Fietz, D. X. Fischer, E. Gaio, L. Giannini, F. Giorgetti, R. Heller, I. Ivashov, B. Lacroix, M. Lewandowska, A. Maistrello, L. Morici, L. Muzzi, A. Nijhuis, F. Nunio, A. Panin, X. Sarasola, L. Savoldi, K. Sedlak, B. Stepanov, G. Tomassetti, A. Torre, S. Turtù, D. Uglietti, R. Vallcorba, K. P. Weiss, R. Wesche, M. J. Wolf, K. Yagotintsev, L. Zani, R. Zanino, Progress in the design of the superconducting magnets for the EU DEMO, Fusion Engineering and Design 136 (September 2017) (2018) 1597–1604. doi:10.1016/j.fusengdes.2018.05.065.

[14] X. Liu, F. Wu, Z. Wang, G. Li, X. Liu, H. Li, J. Li, Y. Ren, Y. Wu, X. Gao, Progress in the conceptual design of the CFETR toroidal field coil with rectangular conductors, Nuclear Fusion 60 (4) (2020) 046032. doi:10.1088/1741-4326/ab742d.

[15] Y. Wu, L. Wang, Anisotropy of the magnetic field of the tf coils in cfetr, Fusion Engineering and Design 143 (2019) 240–246. doi:https://doi.org/10.1016/j.fusengdes.2019.04.004.

[16] X. Sarasola, R. Wesche, I. Ivashov, K. Sedlak, D. Uglietti, P. Bruzzone, Progress in the design of a hybrid hts-nb3sn-nbti central solenoid for the eu demo, IEEE Transactions on Applied Superconductivity 30 (4) (2020) 1–5. doi:10.1109/TASC.2020.2965066.

[17] M. Kovari, R. Kemp, H. Lux, P. Knight, J. Morris, D. Ward, "process": A systems code for fusion power plants—part 1: Physics, Fusion Engineering and Design 89 (12) (2014) 3054–3069. doi:https://doi.org/10.1016/j.fusengdes.2014.09.018.

[18] F. Franza, L. Boccaccini, U. Fisher, P. Gade, R. Heller, On the implementation of new technology modules for fusion reactor systems codes, Fusion Engineering and Design 98-99 (2015) 1767–1770, proceedings of the 28th Symposium On Fusion Technology (SOFT-28). doi:https://doi.org/10.1016/j.fusengdes.2015.03.034.

[19] M. Coleman, S. McIntosh, BLUEPRINT: A novel approach to fusion reactor design, Fusion Engineering and Design 139 (October 2018) (2019) 26–38. doi:10.1016/j.fusengdes.2018.12.036.

[20] S. C. Jardin, C. E. Kessel, J. Menard, T. K. Mau, R. Miller, F. Najmabadi, V. S. Chan, L. L. Lao, Y. R. Linliu, R. L. Miller, T. Petrie, P. A. Politzer, A. D. Turnbull, Physics basis for a spherical torus power plant,

Fusion Engineering and Design 65 (2) (2003) 165–197. doi:10.1016/S0920-3796(02)00303-4.

[21] J. E. Menard, R. Majeski, M. Ono, N. N. Bakharev, V. K. Gusev, M. Gryaznevich, D. Kingham, S. McNamara, P. Thomas, K. Hanada, J. Harrison, B. Lloyd, Y. S. Hwang, B. Lipschultz, H. Wilson, Y. Nagayama, Y. Ono, Y. Takase, M. Reinke, K. Tobita, Z. Gao, F. Alladio, R. J. Fonck, Fusion Energy Development Applications Utilizing the Spherical Tokamak and Associated Research Needs and Tools, IAEA Fusion Energy Conference 27th (IAEA-CN-258) (2018) OV/P–6.

[22] ITER Organisation, Plant Description Document, 2001.
URL `https://www.fusion.qst.go.jp/ITER/FDR/PDD/index.htm`

[23] K. Ioki, V. Barabash, C. Bachmann, P. Chappuis, C. Choi, J.-J. Cordier, B. Giraud, Y. Gribov, P. Heitzenroeder, G. Johnson, L. Jones, C. Jun, B. Kim, E. Kuzmin, D. Loesser, A. Martin, J.-M. Martinez, M. Merola, H. Pathak, P. Readman, M. Sugihara, A. Terasawa, Y. Utin, X. Wang, S. Wu, Iter vacuum vessel design and construction, Fusion Engineering and Design 85 (7) (2010) 1307 – 1313, proceedings of the Ninth International Symposium on Fusion Nuclear Technology. doi:10.1016/j.fusengdes.2010.03.027.

[24] A. N. Mauer, W. M. Stacey, J. Mandrekas, E. A. Hoffman, A Superconducting Tokamak Fusion Transmutation of Waste Reactor, Fusion Science and Technology 45 (1) (2004) 55–59. doi:10.13182/FST04-A426.

[25] T. Hayashi, K. Tobita, Y. Nakamori, S. Orimo, Advanced neutron shielding material using zirconium borohydride and zirconium hydride, Journal of Nuclear Materials 386-388 (C) (2009) 119–121. doi:10.1016/j.jnucmat.2008.12.073.

[26] C. G. Windsor, J. G. Morgan, Neutron and gamma flux distributions and their implications for radiation damage in the shielded superconducting core of a fusion power plant, Nuclear Fusion 57 (2017) 116032. doi:10.1088/1741-4326/aa7e3e.

[27] L. El-Guebaly, M. Harb, A. Davis, J. Menard, T. Brown, ST-based fusion nuclear science facility: Breeding issues and challenges of protecting HTS magnets, Fusion Science and Technology 72 (3) (2017) 354–361. doi:10.1080/15361055.2017.1333864.

[28] B. Colling, Blanket performance and radioactive waste of fusion reactors: a neutronics approach, Ph.D. thesis, Lancaster University (Oct. 2019). doi:10.17635/lancaster/thesis/744.

[29] C. G. Windsor, J. O. Astbury, J. J. Davidson, C. J. McFadzean, J. G. Morgan, C. L. Wilson, S. A. Humphry-Baker, Tungsten boride shields in a spherical tokamak fusion power plant, Nuclear Fusion 61 (8) (2021) 086018. doi:10.1088/1741-4326/ac09ce.

[30] R. T. Santoro, Radiation shielding for fusion reactors, Journal of Nuclear Science and Technology 37 (sup1) (2000) 11–18. doi:10.1080/00223131.2000.10874838.

[31] M. A. Abdou, Radiation considerations for superconducting fusion magnets, Journal of Nuclear Materials 72 (1-2) (1978) 147–167. doi:10.1016/0022-3115(78)90398-7.

[32] H. W. Weber, Radiation Effects on Superconducting Fusion Magnet Components, International Journal of Modern Physics E 20 (06) (2011) 1325–1378. doi:10.1142/S0218301311018526.

[33] S. Haindl, M. Eisterer, R. Müller, R. Prokopec, H. W. Weber, M. Müller, H. Kirchmayr, T. Takeuchi, L. Bargioni, Neutron irradiation effects on A15 multifilamentary wires, IEEE Transactions on Applied Superconductivity 15 (2 PART III) (2005) 3414–3417. doi:10.1109/TASC.2005.848950.

[34] D. X. Fischer, R. Prokopec, J. Emhofer, M. Eisterer, The effect of fast neutron irradiation on the superconducting properties of REBCO coated conductors with and without artificial pinning centers, Superconductor Science and Technology 31 (4) (2018) 044006. doi:10.1088/1361-6668/aaadf2.

[35] J. Hourtoule, C. Neumeyer, I. Suh, Y. Ding, L. Dong, C. Boyer, D. C. Rodrigues, ITER electrical distribution system, 2013 IEEE 25th Symposium on Fusion Engineering, SOFE 2013 (2013). doi:10.1109/SOFE.2013.6635314.

[36] J.-L. L. Duchateau, P. Hertout, B. Saoutic, J.-F. F. Artaud, L. Zani, C. Reux, Conceptual integrated approach for the magnet system of a tokamak reactor, Fusion Engineering and Design 89 (11) (2014) 2606–2620. doi:10.1016/j.fusengdes.2014.06.012.

[37] E. Monneret, M. Chalifour, M. Bonneton, E. Fauve, T. Voigt, S. Badgujar, H. S. Chang, G. Vincent, ITER cryoplant status and economics of the LHe plants, Physics Procedia 67 (2015) 35–41. doi:10.1016/j.phpro.2015.06.007.
URL http://dx.doi.org/10.1016/j.phpro.2015.06.007

[38] S. Minucci, S. Panella, S. Ciattaglia, M. C. Falvo, A. Lampasi, Electrical loads and power systems for the DEMO nuclear fusion project, Energies 13 (9) (2020) 1–21. doi:10.3390/en13092269.

[39] M. Roberto, R. M. Galvao, 'Natural elongation' of spherical tokamaks, Nuclear Fusion 32 (9) (1992) 1666–1669. doi:10.1088/0029-5515/32/9/I17.

[40] J. E. Menard, S. C. Jardin, S. M. Kaye, C. E. Kessel, J. Manickam, Ideal MHD stability limits of low aspect ratio tokamak plasmas, Nuclear Fusion 37 (5) (1997) 595–610. doi:10.1088/0029-5515/37/5/I03.

[41] R. L. Miller, Y. R. Lin-Liu, A. D. Turnbull, V. S. Chan, L. D. Pearlstein, O. Sauter, L. Villard, Stable equilibria for bootstrap-current-driven low aspect ratio tokamaks, Physics of Plasmas 4 (4) (1997) 1062–1068. doi:10.1063/1.872193.
URL https://doi.org/10.1063/1.872193

[42] T. Hender, R. Akers, S. Allfrey, A. Bond, G. Counsell, M. Gryaznevich, P. J. Knight, G. P. Maddison, K. McClements, K. Morel, C. M. Roach, D. C. Robinson, G. Voss, H. R. Wilson, The Physics of Spherical Tokamak Power Plant Designs, in: EPS Conference on Controlled Fusion and Plasma Physics, Vol. 23J, Maastricht, 1999, pp. 229–232.

[43] M. C. R. Andrade, G. O. Ludwig, Scaling of bootstrap current on equilibrium and plasma profile parameters in tokamak plasmas, Plasma Physics and Controlled Fusion 50 (6) (2008) 065001. doi:10.1088/0741-3335/50/6/065001.

[44] R. M. O. Galvao, S. G. Kalmykov, M. Roberto, W. P. de Sa, Dependence of Natural Elongation of Low-Aspect-Ratio Tokamak Plasmas on Current Profile, Comments on Plasma Physics and Controlled Fusion 15 (4) (1993) 219–226.

[45] S. G. Kalmykov, Low-Aspect-Ratio Tokamaks: Plasma Sheath Cross Section Natural Elongation as a Function of Current Density Profile, Plasma Physics Reports 20 (10) (1994) 844–845.

[46] C. G. Bathke, D. A. Ehst, H. Y. Khater, F. Najmabadi, I. N. Sviatoslavsky, P. Titus, M. Billone, L. A. El-guebaly, C. E. Kessel, M. Sidorov, D.-k. Sze, L. Bromberg, S. C. Jardin, T.-k. Mau, D. Steiner, M. S. Tillack, C. P. C. Wong, 8. Assessment of low-aspect-ratio tokamak power plant, in: The Starlite Study: Assessment of Options for Tokamak Power Plants, 1997.

[47] F. Li, J. Zhang, Q. Gao, Z. Wang, W. Xu, Natural Shaping of Spherical Tokamak Plasma, Journal of Plasma Fusion Research 1 (1998) 522–525.

[48] R. J. Akers, A. Bond, R. J. Buttery, P. G. Carolan, G. F. Counsell, G. Cunningham, S. J. Fielding, C. G. Gimblett, M. Gryaznevich, R. J. Hastie, P. Helander, T. C. Hender, P. J. Knight, C. N. Lashmore-Davies, G. P. Maddison, T. J. Martin, K. G. McClements, A. W. Morris, M. R. O'Brien, C. Ribeiro, C. M. Roach, D. C. Robinson, A. Sykes, G. M. Voss, M. J. Walsh, H. R. Wilson, F. S. Zaitsev, Steady state operation of spherical tokamaks, Nuclear Fusion 40 (6) (2000) 1223–1244. doi:10.1088/0029-5515/40/6/317.

[49] R. Aymar, P. Barabaschi, Y. Shimomura, The ITER design, Plasma Physics and Controlled Fusion 44 (2002) 519–565. arXiv:1011.1669.

[50] R. Buttery, R. Akers, E. Arends, N. Conway, G. Counsell, G. Cunningham, C. Gimblett, M. Gryaznevich, R. Hastie, M. Hole, I. Lehane, R. Martin, A. Patel, T. Pinfold, O. Sauter, D. Taylor, G. Turri, M. Valovic, M. Walsh, H. Wilson, the MAST team, Stability at high performance in the MAST spherical tokamak, Nuclear Fusion 44 (9) (2004) 1027–1035. doi:10.1088/0029-5515/44/9/012.

[51] J. Snape, Experimental studies of neoclassical tearing modes on the MAST spherical tokamak, Phd, University of York (2012).

[52] M. Valovič, H. Meyer, R. Akers, C. Brickley, N. Conway, G. Cunningham, A. Kirk, B. Lloyd, A. Patel, D. Taylor, M. Walsh, the MAST Team, Energy and particle confinement in MAST, Nuclear Fusion 45 (8) (2005) 942–949. doi:10.1088/0029-5515/45/8/023.

[53] F. Wagner, The physics basis of iter confinement, AIP Conference Proceedings 1095 (1) (2009) 31–53. doi:10.1063/1.3097319.

[54] S. P. Gerhardt, D. A. Gates, S. M. Kaye, R. Maingi, J. E. Menard, S. A. Sabbagh, V. Soukhanovskii, M. G. Bell, R. E. Bell, J. M. Canik, E. Fredrickson, R. Kaita, E. Kolemen, H. Kugel, B. P. Le Blanc, D. Mastrovito, D. Mueller, H. Yuh, Recent progress towards an advanced spherical torus operating point in NSTX, Nuclear Fusion 51 (7) (2011). doi:10.1088/0029-5515/51/7/073031.

[55] ITER Physics Expert Groups on Confinement and Transport, ITER Physics Expert Groups on Confinement and Transport and Confinement Modelling and Database, Chapter 2: Plasma confinement and transport ITER, Nuclear Fusion 39 (1999) 2175.

[56] A. C. Sips, J. Schweinzer, T. C. Luce, S. Wolfe, H. Urano, J. Hobirk, S. Ide, E. Joffrin, C. Kessel, S. H. Kim, P. Lomas, I. Nunes, T. Pütterich, F. Rimini, W. M. Solomon, J. Stober, F. Turco, P. C. De Vries, J. Contributors, T. A. U. Team, T. D.-D. Team, T. C.-M. Team, T. J.-U. Team, ITPA-IOS TG members and experts, Assessment of the baseline scenario at $q_{95} \circ 3$ for ITER, Nuclear Fusion 58 (12) (2018). doi:10.1088/1741-4326/aade57.

[57] M. Valovič, R. Akers, G. Cunningham, L. Garzotti, B. Lloyd, D. Muir, A. Patel, D. Taylor, M. Turnyanskiy, M. Walsh, Scaling of H-mode energy confinement with Ip and BT in the MAST spherical tokamak, Nuclear Fusion 49 (7) (2009) 075016. doi:10.1088/0029-5515/49/7/075016.

[58] P. F. Buxton, J. W. Connor, A. E. Costley, M. P. Gryaznevich, S. McNamara, On the energy confinement time in spherical tokamaks: implications for the design of pilot plants and fusion reactors, Plasma Physics and Controlled Fusion 61 (3) (2019) 035006. doi:10.1088/1361-6587/aaf7e5.

[59] G. Verdoolaege, S. Kaye, C. Angioni, O. Kardaun, M. Maslov, M. Romanelli, F. Ryter, K. Thomsen, T. ASDEX Upgrade Team, T. EUROfusion MST1 Team, J. Contributors, The updated ITPA global H-mode confinement database: description and analysis, Nuclear Fusion 61 (7) (2021) 076006. doi:10.1088/1741-4326/abdb91.

[60] C. Fausser, A. L. Puma, F. Gabriel, R. Villari, Tokamak D-T neutron source models for different plasma physics confinement modes, Fusion Engineering and Design 87 (5-6) (2012) 787–792. doi:10.1016/j.fusengdes.2012.02.025.

[61] R. Dendy (Ed.), Plasma Physics: An Introductory Course, Cambridge University Press, 1993.

[62] F. Troyon, R. Gruber, H. Saurenmann, S. Semenzato, S. Succi, MHD-limits to plasma confinement, Plasma Physics and Controlled Fusion 26 (1A) (1984) 209–215. doi:10.1088/0741-3335/26/1a/319.

[63] F. Troyon, A. Roy, W. A. Cooper, F. Yasseen, A. Turnbull, Beta limit in tokamaks. experimental and computational status, Plasma Physics and Controlled Fusion 30 (11) (1988) 1597–1609. doi:10.1088/0741-3335/30/11/019.

[64] M. F. T. A. Sykes A, S. Patel, in: Proc. 11th Eur. Conf. Controlled Fusion and Plasma Physics, Vol. 2, 1983, p. 363.

[65] A. Sykes, R. Akers, L. Appel, P. G. Carolan, N. J. Conway, M. Cox, A. R. Field, D. A. Gates, S. Gee, M. Gryaznevich, T. C. Hender, I. Jenkins, R. Martin, K. Morel, A. W. Morris, M. P. S. Nightingale, C. Ribeiro, D. C. Robinson, M. Tournianski, M. Valovic, M. J. Walsh, C. Warrick, High- performance of the START spherical tokamak, Plasma Physics and Controlled Fusion 39 (12B) (1997) B247–B260. doi:10.1088/0741-3335/39/12b/019.

[66] E. Synakowski, M. Bell, R. Bell, T. Bigelow, M. Bitter, W. Blanchard, J. Boedo, C. Bourdelle, C. Bush, D. Darrow, P. Efthimion1, E. Fredrickson, D. Gates, M. Gilmore, L. Grisham, J. Hosea, D. Johnson, R. Kaita, S. Kaye, S. Kubota, H. Kugel, B. LeBlanc, K. Lee, R. Maingi, J. Manickam, R. Maqueda, E. Mazzucato, S. Medley, J. Menard, D. Mueller, B. Nelson, C. Neumeyer, M. Ono, F. Paoletti, H. Park, S. Paul, Y.-K. Peng, C. Phillips, S. Ramakrishnan, R. Raman, A. Roquemore, A. Rosenberg, P. Ryan, S. Sabbagh, C. Skinner, V. Soukhanovskii, T. Stevenson, D. Stutman, D. Swain, G. Taylor, A. V. Halle, J. Wilgen, M. Williams, J. Wilson, S. Zweben, R. Akers, R. Barry, P. Beiersdorfer, J. Bialek, B. Blagojevic, P. Bonoli, R. Budny, M. Carter, C. Chang, J. Chrzanowski, W. Davis, B. Deng, E. Doyle, L. Dudek, J. Egedal, R. Ellis, J. Ferron, M. Finkenthal, J. Foley, E. Fredd, A. Glasser, T. Gibney, R. Goldston, R. Harvey, R. Hatcher, R. Hawryluk, W. Heidbrink, K. Hill, W. Houlberg, T. Jarboe, S. Jardin, H. Ji, M. Kalish, J. Lawrance, L. Lao, K. Lee,

F. Levinton, N. Luhmann, R. Majeski, R. Marsala, D. Mastravito, T. Mau, B. McCormack, M. Menon, O. Mitarai, M. Nagata, N. Nishino, M. Okabayashi, G. Oliaro, D. Pacella, R. Parsells, T. Peebles, B. Peneflor, D. Piglowski, R. Pinsker, G. Porter, A. Ram, M. Redi, M. Rensink, G. Rewoldt, J. Robinson, P. Roney, M. Schaffer, K. Shaing, S. Shiraiwa, P. Sichta, D. Stotler, B. Stratton, Y. Takase, X. Tang, R. Vero, W. Wampler, G. Wurden, X. Xu, J. Yang, L. Zeng, W. Zhu, The national spherical torus experiment (NSTX) research programme and progress towards high beta, long pulse operating scenarios, Nuclear Fusion 43 (12) (2003) 1653–1664. doi:10.1088/0029-5515/43/12/011.

[67] S. Sabbagh, J.-W. Ahn, J. Allain, R. Andre, A. Balbaky, R. Bastasz, D. Battaglia, M. Bell, R. Bell, P. Beiersdorfer, E. Belova, J. Berkery, R. Betti, J. Bialek, T. Bigelow, M. Bitter, J. Boedo, P. Bonoli, A. Boozer, A. Bortolon, D. Boyle, D. Brennan, J. Breslau, R. Buttery, J. Canik, G. Caravelli, C. Chang, N. Crocker, D. Darrow, B. Davis, L. Delgado-Aparicio, A. Diallo, S. Ding, D. D'Ippolito, C. Domier, W. Dorland, S. Ethier, T. Evans, J. Ferron, M. Finkenthal, J. Foley, R. Fonck, R. Frazin, E. Fredrickson, G. Fu, D. Gates, S. Gerhardt, A. Glasser, N. Gorelenkov, T. Gray, Y. Guo, W. Guttenfelder, T. Hahm, R. Harvey, A. Hassanein, W. Heidbrink, K. Hill, Y. Hirooka, E. Hooper, J. Hosea, D. Humphreys, K. Indireshkumar, F. Jaeger, T. Jarboe, S. Jardin, M. Jaworski, R. Kaita, J. Kallman, O. Katsuro-Hopkins, S. Kaye, C. Kessel, J. Kim, E. Kolemen, G. Kramer, S. Krasheninnikov, S. Kubota, H. Kugel, R. L. Haye, L. Lao, B. LeBlanc, W. Lee, K. Lee, J. Leuer, F. Levinton, Y. Liang, D. Liu, J. Lore, N. Luhmann, R. Maingi, R. Majeski, J. Manickam, D. Mansfield, R. Maqueda, E. Mazzucato, A. McLean, D. McCune, B. McGeehan, G. McKee, S. Medley, E. Meier, J. Menard, M. Menon, H. Meyer, D. Mikkelsen, G. Miloshevsky, D. Mueller, T. Munsat, J. Myra, B. Nelson, N. Nishino, R. Nygren, M. Ono, T. Osborne, H. Park, J. Park, Y. Park, S. Paul, W. Peebles, B. Penaflor, R. Perkins, C. Phillips, A. Pigarov, M. Podesta, J. Preinhaelter, R. Raman, Y. Ren, G. Rewoldt, T. Rognlien, P. Ross, C. Rowley, E. Ruskov, D. Russell, D. Ruzic, P. Ryan, M. Schaffer, E. Schuster, F. Scotti, K. Shaing, V. Shevchenko, K. Shinohara, V. Sizyuk, C. Skinner, A. Smirnov, D. Smith, P. Snyder, W. Solomon, A. Sontag, V. Soukhanovskii, T. Stoltzfus-Dueck, D. Stotler, B. Stratton, D. Stutman, H. Takahashi, Y. Takase, N. Tamura, X. Tang, G. Taylor, C. Taylor, K. Tritz, D. Tsarouhas, M. Umansky, J. Urban, E. Untergberg, M. Walker, W. Wampler, W. Wang, J. Whaley, R. White, J. Wilgen, R. Wilson, K. Wong, J. Wright, Z. Xia, D. Youchison, G. Yu, H. Yuh, L. Zakharov, D. Zemlyanov, G. Zimmer, S. Zweben, Overview of physics results from the conclusive operation of the national spherical torus experiment, Nuclear Fusion 53 (10) (2013) 104007. doi:10.1088/0029-5515/53/10/104007.

[68] J. Berkery, S. Sabbagh, A. Thornton, A. Kirk, L. Kogan, J. Hollocombe, Disruptivity and Density Limits in MAST and other Tokamaks, in: APS

Division of Plasma Physics Meeting Abstracts, Vol. 2018 of APS Meeting Abstracts, 2018, p. CP11.095.

[69] E. Poli, G. Tardini, H. Zohm, E. Fable, D. Farina, L. Figini, N. Marushchenko, L. Porte, Electron-cyclotron-current-drive efficiency in DEMO plasmas, Nuclear Fusion 53 (1) (2012) 013011. doi:10.1088/0029-5515/53/1/013011.
URL https://doi.org/10.1088/0029-5515/53/1/013011

[70] D. R. Mikkelsen, C. E. Kessel, F. M. Poli, N. Bertelli, K. Kim, Survey of heating and current drive for K-DEMO, Nuclear Fusion 58 (3) (2018). doi:10.1088/1741-4326/aaa4d2.

[71] L. Bromberg, M. Tekula, L. El-Guebaly, R. Miller, Options for the use of high temperature superconductor in tokamak fusion reactor designs, Fusion Engineering and Design 54 (2) (2001) 167–180. doi:https://doi.org/10.1016/S0920-3796(00)00432-4.

[72] Y. Zhai, C. Kessel, L. El-Guebaly, P. Titus, Magnet design considerations for fusion nuclear science facility, IEEE Transactions on Applied Superconductivity 26 (4) (2016) 1–5. doi:10.1109/TASC.2016.2532921.

[73] C. Windsor, J. Marshall, J. Morgan, J. Fair, G. Smith, A. Rajczyk-Wryk, J. Tarragó, Design of cemented tungsten carbide and boride-containing shields for a fusion power plant, Nuclear Fusion 58 (7) (2018) 076014. doi:10.1088/1741-4326/aabdb0.

[74] C. A. Phillips, Princeton plasma physics laboratory annual report, october 1, 1983-september 30, 1984doi:10.2172/6002368.
URL https://www.osti.gov/biblio/6002368

[75] D. Bartlett, R. Bickerton, M. Brusati, D. Campbell, J. Christiansen, J. Cordey, S. Corti, A. Costley, A. Edwards, J. Fessey, M. Gadeberg, A. Gibson, R. Gill, N. Gottardi, A. Gondhalekar, C. Gowers, F. Hendriks, O. Jarvis, E. Källne, J. Källne, S. Kissel, L. D. Kock, H. Krause, E. Lazzaro, P. Lomas, F. Mast, P. Morgan, P. Nielsen, R. Prentice, R. Ross, J. O'Rourke, G. Sadler, F. Schüller, M. Stamp, P. Stott, D. Summers, A. Tanga, A. Taroni, P. Thomas, F. Tibone, G. Tonetti, B. Tubbing, M. Watkins, Energy confinement in JET ohmically heated plasmas, Nuclear Fusion 28 (1) (1988) 73–88. doi:10.1088/0029-5515/28/1/006.
URL https://doi.org/10.1088/0029-5515/28/1/006

[76] J. D. Huba, NRL PLASMA FORMULARY Supported by The Office of Naval Research, Naval Research Laboratory, Washington, DC, 2013.
URL http://wwwppd.nrl.navy.mil/nrlformulary/

[77] F. Albajar, J. Johner, G. Granata, Improved calculation of synchrotron radiation losses in realistic tokamak plasmas, Nuclear Fusion 41 (6) (2001) 665–678. doi:10.1088/0029-5515/41/6/301.

[78] J. Pamela, A. Bécoulet, D. Borba, J.-L. Boutard, L. Horton, D. Maisonnier, Efficiency and availability driven r&d issues for demo, Fusion Engineering and Design 84 (2) (2009) 194 – 204, proceeding of the 25th Symposium on Fusion Technology. doi:https://doi.org/10.1016/j.fusengdes.2009.02.028.

[79] G. G. Denisov, A. G. Litvak, New Results of Development of Gyrotrons for Plasma Fusion Installations, Tech. rep., International Atomic Energy Agency (IAEA) (2014).

[80] H. Faugel, V. Bobkov, H. Fünfgelder, J. Noterdaeme, A. Messiaen, D. Van Eester, Icrf system efficiency, Fusion Engineering and Design 156 (2020) 111641. doi:10.1016/j.fusengdes.2020.111641.

[81] U. Fantz, C. Hopf, R. Friedl, S. Cristofaro, B. Heinemann, S. Lishev, A. Mimo, Technology developments for a beam source of an nnbi system for demo, Fusion Engineering and Design 136 (2018) 340 – 344, special Issue: Proceedings of the 13th International Symposium on Fusion Nuclear Technology (ISFNT-13). doi:https://doi.org/10.1016/j.fusengdes.2018.02.025.

[82] I. Turner, A. Holmes, Model for a beam driven plasma neutraliser based on iter beam geometry, Fusion Engineering and Design 149 (2019) 111327. doi:10.1016/j.fusengdes.2019.111327.

[83] D. Constable, et al., High Efficiency Klystron Development for Particle Accelerators, in: Proc. of ICFA Advanced Beam Dynamics Workshop on High Luminosity Circular e^+e^- Colliders (eeFACT'16), Daresbury, UK, October 24-27, 2016, no. 58 in ICFA Advanced Beam Dynamics Workshop on High Luminosity Circular e^+e^- Colliders, JACoW, Geneva, Switzerland, 2017, pp. 185–187. doi:10.18429/JACoW-eeFACT2016-WET3AH2.

[84] E. Surrey, Engineering challenges for accelerated fusion demonstrators, Philosophical Transactions of the Royal Society A: Mathematical, Physical and Engineering Sciences 377 (2019) 20170442. doi:10.1098/rsta.2017.0442.

[85] S. Segantin, A. Bersano, N. Falcone, R. Testoni, Exploration of power conversion thermodynamic cycles for arc fusion reactor, Fusion Engineering and Design 155 (2020) 111645. doi:https://doi.org/10.1016/j.fusengdes.2020.111645.

[86] K. Maki, Energy multiplication in high tritium breeding ratio blanket with front breeder zone for fusion reactors, Journal of Nuclear Science and Technology 25 (1) (1988) 72–80. doi:10.1080/18811248.1988.9733557.

[87] C. C. Baker, M. A. Abdou, C. D. Boley, A. E. Bolon, J. N. Brooks, R. G. Clemmer, D. A. Ehst, K. Evans, P. A. Finn, R. E. Fuja, Y. Gohar, J. Jung, W. J. Kann, R. F. Mattas, B. Misra, H. L. Schreyer, D. L.

Smith, H. C. Stevens, L. R. Turner, D. A. De Freece, C. Dillow, G. D. Morgan, C. A. Trachsel, D. Graumann, J. Alcorn, R. E. Fields, R. Prater, J. Kokoszenski, K. Barry, M. Cherry, H. Klumpe, R. W. Conn, G. A. Emmert, I. N. Sviatoslavsky, D. K. Sze, STARFIRE, a commercial tokamak power plant design, Nuclear Engineering and Design 63 (2) (1981) 199–231. doi:10.1016/0029-5493(81)90044-3.

[88] I. Palermo, D. Rapisarda, I. Fernández-Berceruelo, A. Ibarra, Optimization process for the design of the DCLL blanket for the European DEMOnstration fusion reactor according to its nuclear performances, Nuclear Fusion 57 (7) (2017) 076011. doi:10.1088/1741-4326/aa6c14.

[89] ITER Organisation, ITER Technical Basis, Tech. rep. (2002).

[90] G. Zhuang, G. Q. Li, J. Li, Y. X. Wan, Y. Liu, X. L. Wang, Y. T. Song, V. Chan, Q. W. Yang, B. N. Wan, X. R. Duan, P. Fu, B. J. Xiao, Progress of the CFETR design, Nuclear Fusion 59 (2019) 112010. doi:10.1088/1741-4326/ab0e27.

[91] E. Nonbøl, Description of the advanced gas cooled type of reactor (AGR), NKS-RAK-2(96)TR-C2, 1996.

[92] W. E. Cummins, M. M. Corletti, T. L. Schulz, Westinghouse AP1000 advanced passive plant, in: Proceedings of the American Nuclear Society - International Congress on Advances in Nuclear Power Plants 2005, ICAPP'05, Vol. 6, 2005, pp. 3337–3346.

[93] C. English, D. Buckthorpe, Lessons learnt from fission materials R&D programmes, Nuclear Fusion 57 (9) (2017). doi:10.1088/1741-4326/57/9/092010.

[94] F. Schoofs, T. N. Todd, Fusion reactor calculator (2021). doi:10.6084/m9.figshare.16850191.

[95] C. Tarantini, P. J. Lee, N. Craig, A. Ghosh, D. C. Larbalestier, Examination of the trade-off between intrinsic and extrinsic properties in the optimization of a modern internal tin Nb3Sn conductor, Superconductor Science and Technology 27 (6) (2014) 065013. doi:10.1088/0953-2048/27/6/065013.

[96] G. Majkic, R. Pratap, A. Xu, E. Galstyan, H. C. Higley, S. O. Prestemon, X. Wang, D. Abraimov, J. Jaroszynski, V. Selvamanickam, Engineering current density over 5 kA mm-2 at 4.2 K, 14 T in thick film REBCO tapes, Superconductor Science and Technology 31 (2018) 10LT01. doi:10.1088/1361-6668/aad844.

[97] S. Hahn, K. Kim, K. Kim, X. Hu, T. Painter, I. Dixon, S. Kim, K. R. Bhattarai, S. Noguchi, J. Jaroszynski, D. C. Larbalestier, 45.5-tesla direct-current magnetic field generated with a high-temperature superconducting magnet, Nature (2019). doi:10.1038/s41586-019-1293-1.

[98] D. C. van der Laan, J. D. Weiss, D. McRae, Status of CORC® cables and wires for use in high-field magnets and power systems a decade after their introduction, Superconductor Science and Technology 32 (3) (2019) 33001. doi:10.1088/1361-6668/aafc82.

[99] Z. S. Hartwig, R. Vieira, B. N. Sorbom, R. A. Badcock, M. Bajko, W. K. Beck, B. Castaldo, C. L. Craighill, M. Davies, J. Estrada, V. Fry, T. Golfinopoulos, A. E. Hubbard, J. H. Irby, S. Kuznetsov, C. J. Lammi, P. Michael, T. Mouratidis, R. A. Murray, A. T. Pfeiffer, S. Z. Pierson, A. Radovinsky, M. D. Rowell, E. E. Salazar, M. Segal, P. W. Stahle, M. Takayasu, T. L. Toland, L. Zhou, VIPER: An industrially scalable high-current high temperature superconductor cable, Superconductor Science and Technology (2020). doi:https://doi.org/10.1088/1361-6668/abb8c0.

[100] R. Ambrosino, A. Castaldo, S. Ha, V. Loschiavo, S. Merriman, H. Reimerdes, Evaluation of feasibility and costs of alternative magnetic divertor configurations for demo, Fusion Engineering and Design 146 (2019) 2717–2720, sI:SOFT-30. doi:https://doi.org/10.1016/j.fusengdes.2019.04.095.

[101] G. Federici, R. Kemp, D. Ward, C. Bachmann, T. Franke, S. Gonzalez, C. Lowry, M. Gadomska, J. Harman, B. Meszaros, C. Morlock, F. Romanelli, R. Wenninger, Overview of EU DEMO design and R&D activities, Fusion Engineering and Design 89 (7-8) (2014) 882–889. doi:10.1016/j.fusengdes.2014.01.070.